

Short communication

Synthesis of Al and In dual-doped CuO nanostructures via SILAR method: Structural, optical and electrical properties

O. Kahveci^a, A. Akkaya^b, R. Aydın^{c,*}, B. Şahin^d, E. Ayyıldız^a^a Department of Physics, Faculty of Sciences, Erciyes University, Kayseri, Turkey^b Mucur Technical Vocational Schools, Tech. Prog. Department, Kırşehir Ahi Evran University, Kırşehir, Turkey^c Department of Physics, Faculty of Sciences, Selçuk University, Konya, Turkey^d Department of Physics, Faculty of Arts and Sciences, Mustafa Kemal University, Hatay, Turkey

ARTICLE INFO

Keywords:

CuO films
Co-doping
SILAR
Crystallinity
Optical bandgap
Resistivity

ABSTRACT

In this article, we investigated the doping characteristics of Al-doped CuO (ACO), and Al/In co-doped CuO (AICO) thin films, which were synthesized on glass substrates, via the solution-based successive ionic layer adsorption and reaction (SILAR) technique. The surface morphological, chemical composition, structural, optical, and electrical properties of the nanocrystalline films were characterized by Field Emission Scanning Electron Microscopy (FE-SEM), Energy dispersive X-ray spectroscopy (EDX), X-ray diffraction (XRD), Fourier-transform Infrared Spectroscopy (FTIR), Ultraviolet–visible (UV–vis.) spectrophotometry, and Transmission Line Method (TLM), respectively. Surface morphology studies exhibited that a decrease in the films' thickness caused an increment in the optical transmittance. XRD patterns displayed that the obtained samples were polycrystalline and crystallized in a bare CuO monoclinic structure. FTIR studies of the CuO samples displayed that Al and In co-doping influenced the forms and the violence of the absorption bands. The optical bandgap energy of bare CuO was determined to increase from 1.45 to 1.78 eV as a result of the co-doping. The substitution of In displayed in the irregularity of the morphology, owing to its wide ionic radius, which caused an increase in band gap energy and a decrease in resistance. The co-doping of Al and In is hence anticipated to ensure an extensive range of physical and optical properties of nanostructured metal oxide samples for a variety of technological applications.

1. Introduction

Semiconductor metal oxides (SMO), such as CeO₂, SnO₂, ZnO, ZrO, CuO, NiO, and TiO₂ are attractive classes of materials, which are economic and can be fabricated on the scale necessary to meet extensive demand [1–5]. Prominent among these metal oxides is Copper (II) oxide (CuO), also known as cupric oxide due to its nontoxicity, wide-range applicability, abundance in nature and high environmental stability. CuO is a p-type SMO with a narrow band gap of roughly 1.4 eV and high carrier concentration (10¹⁷–10²² cm⁻³) [6–8].

CuO films have a diverse range of implementations in different areas, such as gas sensors, light-emitting diodes, supercapacitors, solar cells, catalysis, electrochromic devices, thin-film transistor, etc., owing to their great electrical, optical, chemical, and physical properties [9–12]. CuO nanoparticles or thin films can be prepared using wide kinds of procedures, namely sputtering, hydrothermal, laser ablation, electrochemical deposition, spray pyrolysis, chemical bath deposition, and

successive ionic layer adsorption and reaction (SILAR) [13–16]. Among these procedures, SILAR is an extremely preferred technique due to its low-cost, simple, safe, and eco-friendly method [17,18].

Doping SMO with another metal is the best method to fine-tune the physical features of the SMO. Doping also modifies the band structures in the SMO. Previous studies on doping of different element ions such as Li, Co, Fe, Al, In, Ce, Zn, etc. into the SMO lattice structure to advance the physical properties of SMO films have been researched [19–21]. Doping with a secondary dopant besides the primary dopant material has been named as 'co-doping'. Co-doping enables the advantages of two dopant materials to be used at the same time. Through this process, the strengths of one dopant element can compensate for a flaw in the other dopant.

Among the elements, Aluminum (Al) is known as a favored dopant element due to its significant advantages, such as abundant minerals, low ionization energy, small ionic radius, low price, low toxicity, and easy availability. Al also displays low resistivity and high transparency

* Corresponding author.

E-mail address: raydin@selcuk.edu.tr (R. Aydın).<https://doi.org/10.1016/j.inoche.2022.110230>

Received 4 September 2022; Received in revised form 10 November 2022; Accepted 16 November 2022

Available online 20 November 2022

1387-7003/© 2022 Elsevier B.V. All rights reserved.

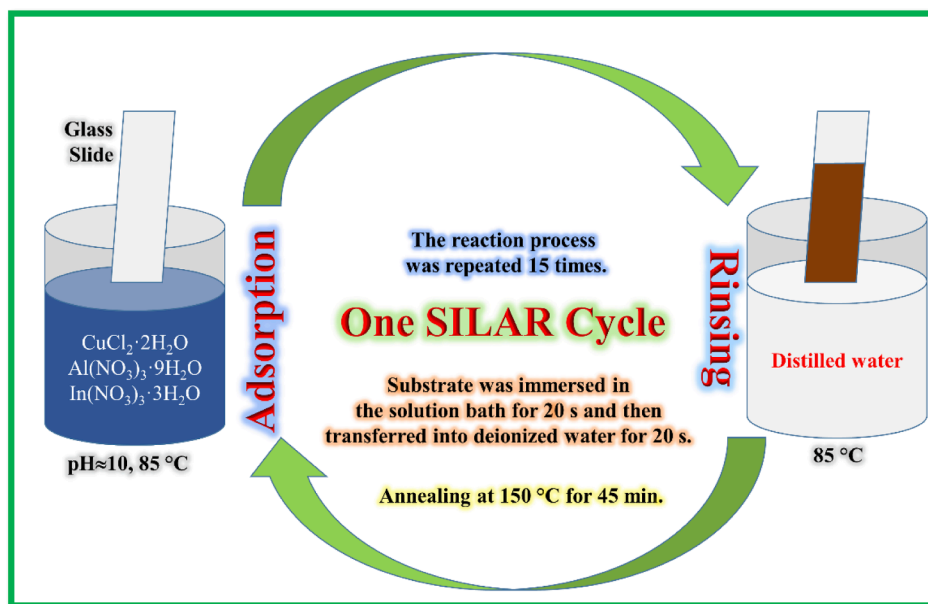


Fig. 1. Schematic illustration of experimental setup of SILAR procedure for deposition of CuO, ACO and AICO films.

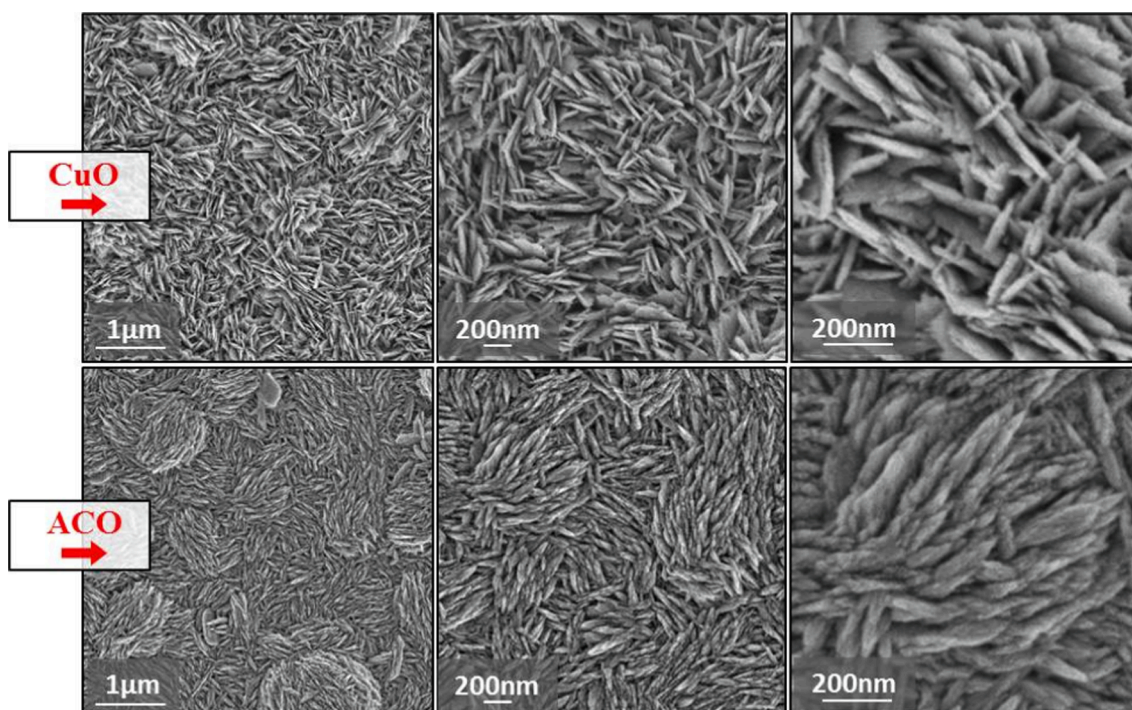


Fig. 2. FE-SEM images of un-doped and Al-doped CuO films.

[22,23]. Indium (In) is a significant dopant material used to alter the optical and electrical properties of SMO films due to its particular features, like mobility, diverse oxidation cases (In^{+3} , In^{+1} , and In^0) trapping, and more electron production. It also possesses a big ionic radius, displaying that the diffusivity of In is the smallest [24,25].

To the best of our knowledge, the influences of Al and In co-doping in CuO films by using the SILAR technique have not been recorded yet. Therefore, in this research, we inform the deposition of bare CuO, Al-doped CuO (ACO), and Al/In co-doped CuO (AICO) films prepared by the SILAR technique. The goal of this work was to examine the influences of Al and In co-doping on the surface morphological, structural, optical, and electrical characteristics of CuO nanostructures.

2. Experimental details

The analytical chemicals, such as copper (II) chloride dihydrate ($\text{CuCl}_2 \cdot 2\text{H}_2\text{O}$, $\geq 99.0\%$ purity), aluminum nitrate nonahydrate ($\text{Al}(\text{NO}_3)_3 \cdot 9\text{H}_2\text{O}$, greater than 99 % purity), and indium nitrate trihydrate ($\text{In}(\text{NO}_3)_3 \cdot 3\text{H}_2\text{O}$, 99.9 % purity) were purchased from the commercial supplier, Sigma-Aldrich and were used to deposit the high-quality CuO, ACO, and AICO films, respectively. In the experiments, acetone (CH_3COCH_3), sulfuric acid (H_2SO_4), and distilled water were used to clean the glass slides and beakers. In addition, ammonium hydroxide solution (NH_4OH) was used to adjust the pH of the reaction bath.

In this experiment, CuO, ACO, and AICO films were prepared on both

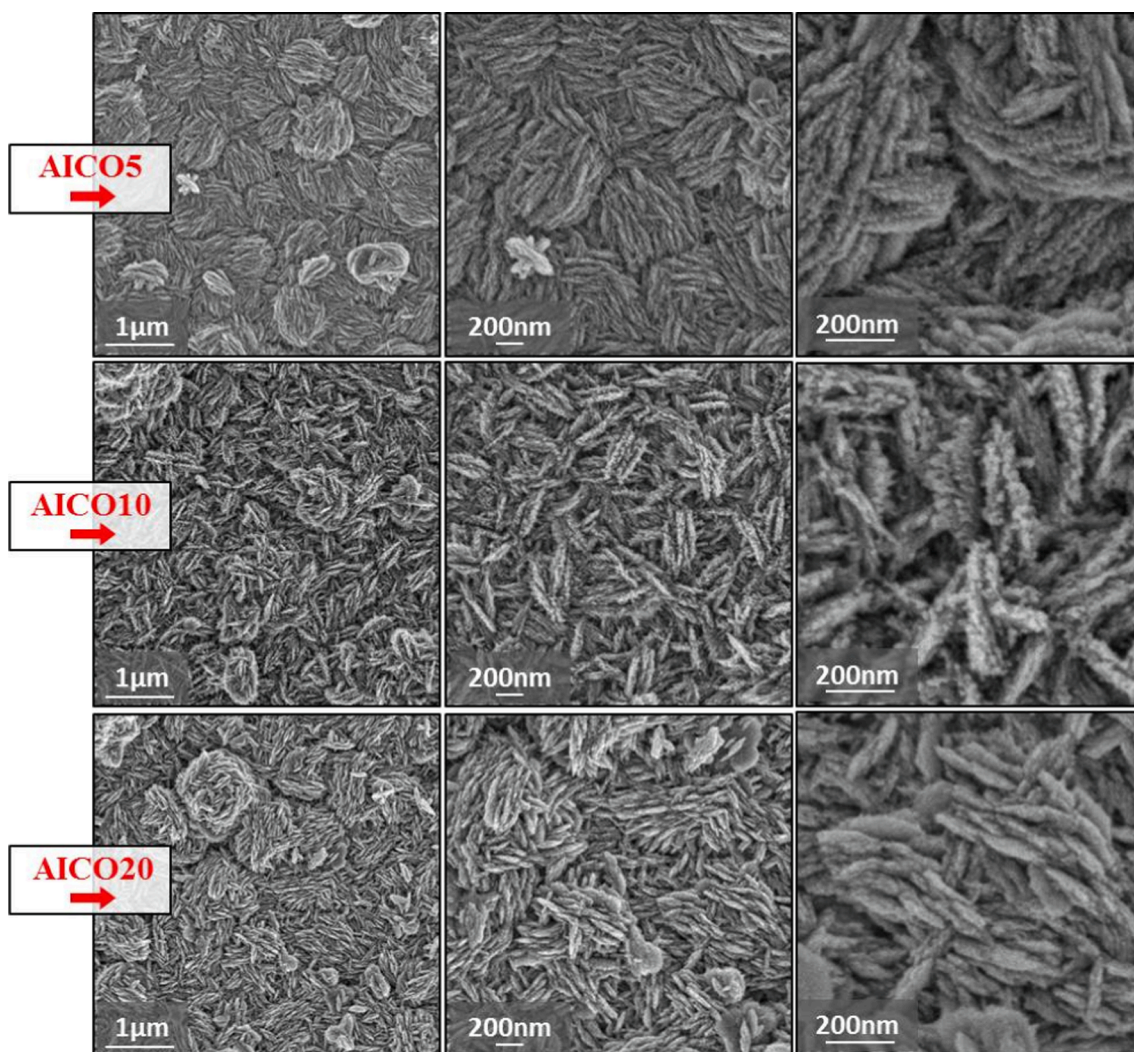


Fig. 3. FE-SEM images of Al/In co-doped CuO films.

sides of the soda-lime glass as substrate by the SILAR route. For the deposit of CuO films, 0.1 M $\text{CuCl}_2 \cdot 2\text{H}_2\text{O}$ dissolved in 100 ml of distilled water was used as a precursor of the Cu^{2+} ion. The pH of the reaction bath was regulated to 10 using NH_4OH and the temperature of the reaction bath was arranged to 85° . A typical SILAR cycle includes sub-jacent steps: First, the substrates were vertically submerged into a 0.1 M CuCl_2 aqueous solution including Cu^{2+} ions for 20 s to adsorb Cu^{2+} ions onto the substrate. Then the substrates were vertically immersed in distilled water to remove weakly bonded Cu^{2+} impurities. This reaction process was iterated for 15 periods to obtain uniform synthesized CuO films. A similar procedure was repeated for ACO and AICO films for 15 cycles to obtain the intended film thickness. Finally, the obtained CuO, ACO, and AICO films were annealed at 150°C for 45 min. Fig. 1 shows the schematic of the deposition process of CuO, ACO, and AICO films. The films were labeled according to the Al^{3+} and In^{3+} doping ratio, that is, ACO (Al: 0.5 %), AICO5 (Al: 0.5 %, and In: 0.5 %), AICO10 (Al: 0.5 % and In: 1.0 %), and AICO20 (Al: 0.5 % and In: 2.0 %).

A Pan Analytical Inc. X-ray diffraction (XRD) unit was used to carry out using Cu (K-alpha) radiation in an X-ray diffractometer to analyze the structure of the CuO, ACO, and AICO films. A Zeiss Gemini 500 Field Emission Scanning Electron Microscopy (FE-SEM) unit was used to examine the morphological properties of the produced films. The elemental composition analysis was designated by using energy dispersive spectrometry (EDX). A Perkin Elmer 400 FT-IR/FT-FIR Spectrometer Spotlight 400 Imaging System carried out the Fourier

Transform Infrared (FTIR) spectroscopy study of the CuO, ACO, and AICO films at room temperature. The optical transmittance and band gap study of the CuO, ACO, and AICO films at room temperature was carried out by a GENESYS 10S UV-vis spectrophotometer (Thermo Scientific). Electrical contacts were made by thermally evaporated high-purity gold. During the thermal evaporation, background pressure was better than 10^{-6} Torr and the evaporation rate was 1.5 \AA/s . Pad dimensions were $3.5 \text{ mm} \times 0.7 \text{ mm}$ (L \times W) and distances between the pads were 0.25 mm, 0.50 mm, and 0.75 mm. Electrical measurements (I-V) were accomplished via computer-controlled Agilent B2912A SMU, at room temperature, and in the dark. Data processing was performed via VEE Pro-based SeCLaS software [26,27].

3. Results and discussions

3.1. Surface morphological and chemical analysis

Fig. 2 shows the surface morphology of un-doped and 0.5 % Al-doped CuO films. Plate-like structures are observed in un-doped CuO film images [28]. As seen in Fig. 2, while plate-like structures are observed in un-doped CuO film images, the structures become plump and have a less rough surface with 0.5 % Al doping. As the form and the shape of the particles in the film structure depend on different effects, such as nucleation and crystal growth rate [29], it appears that Al has a significant effect on the shape and morphology of CuO films. The Al doped

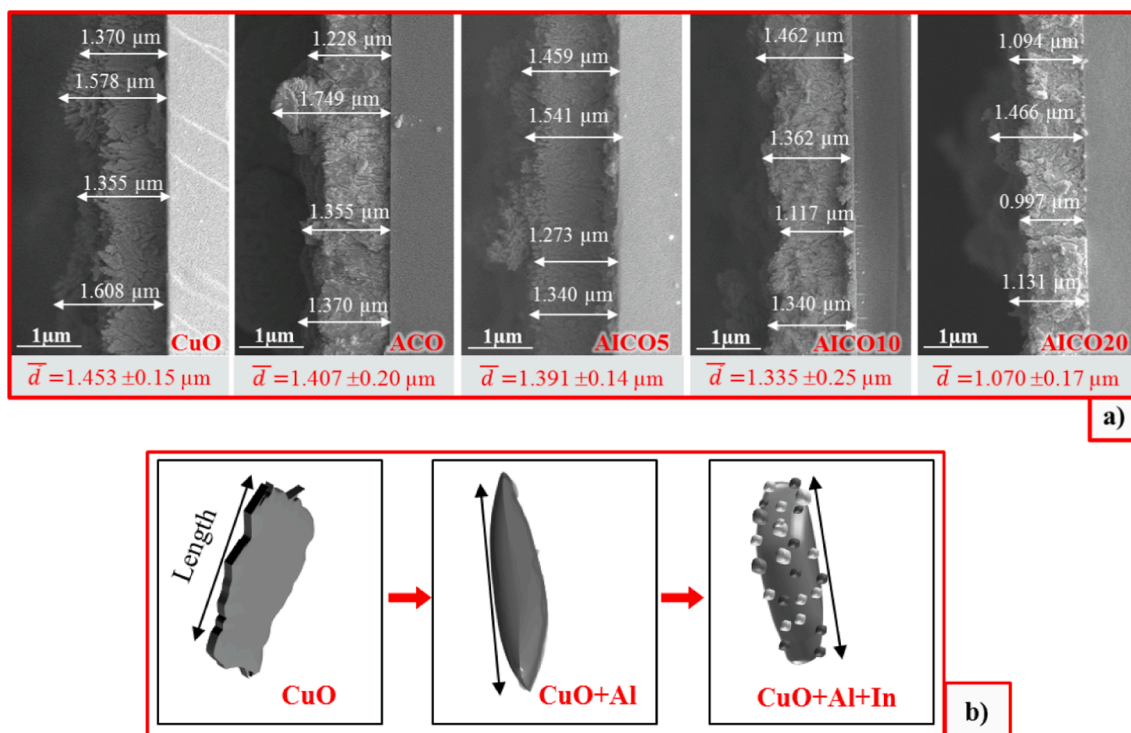


Fig. 4. A) Cross-sectional FE-SEM images of un-doped, Al doped, and Al-In doped CuO films, b) Schematic illustration of changes in CuO nanoparticles' shape by doping.

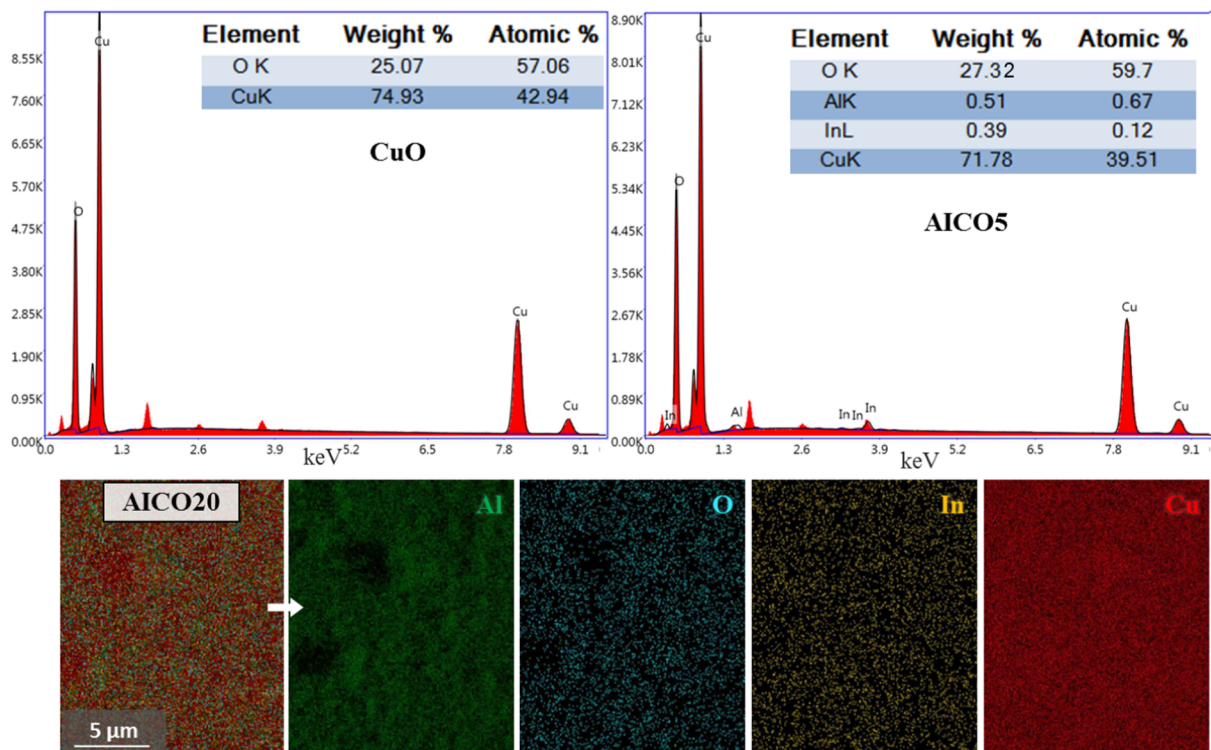


Fig. 5. FESEM-EDX analysis results of CuO, ACO (Al: 0.5 %) and FESEM-mapping images of AICO20 (Al: 0.5 % and In: 2.0 %).

CuO film surface has a relatively smoother morphology. In addition, the lengths of the structures in the films were calculated by taking measurements from the FE-SEM images. The average length of the plate-like structure was 229.7 ± 47.8 nm for un-doped and 228.2 ± 48.5 nm for 0.5 % Al-doped CuO films.

FE-SEM images of dual-doped CuO films with Al and In can be seen in Fig. 3. The particle morphology and shape of the samples changed with the Al/In co-doping.

This adjustment in structure and morphology may be a consequence of the distinctive electronegativity of host metal and dopant

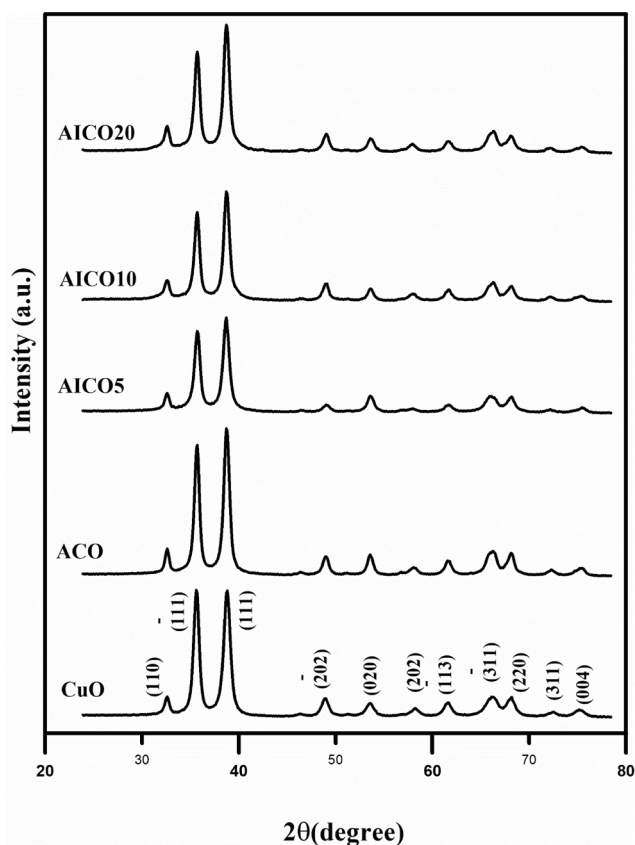


Fig. 6. XRD spectrum of CuO, ACO and AICO films prepared by SILAR method.

Table 1

Relative peak intensity, crystallite size and bandgap values of CuO, ACO and AICO films.

Sample Name	Recorded Peak Intensity		Crystallite Size (nm)	Bandgap (eV)
	($\bar{1}11$)	(111)		
CuO	1732	1724	12.83	1.45
ACO	1783	2009	15.10	1.65
AICO5	1124	1307	13.85	1.69
AICO10	1225	1507	14.10	1.74
AICO20	1390	1751	14.65	1.78

materials, which influences the nucleation process and crystallinity quality of the nanostructured SMO [30,31]. The average length of the structures was measured as 228.6 ± 44.1 nm for AICO5, 228.1 ± 33.8 nm for AICO10, and 223.2 ± 29.7 nm for AICO20.

Fig. 4a shows cross-sectional FE-SEM images for un-doped, Al doped, and Al/In co-doped CuO thin films deposited on a soda-lime glass substrate. According to the cross-sectional images, the maximum average film thickness of the CuO films is 1.453 ± 0.15 μm , and the least average film thickness is 1.070 ± 0.17 μm for the AICO20 film. Average thicknesses were obtained by taking at least ten different measurements from each sample. Considering the dual-doped samples, the film thickness decreases as the In content increases. Fig. 4b shows a schematic illustration of changes in the CuO nanoparticles' shape with Al and In doping. The figure can represent a summary of shape change for Al-doping and Al/In dual-doping. Therefore, the doping process does not significantly affect the length of the structures but rather changes the shape and surface of the structures.

To verify the entity of Al, In, O, and Cu in the samples, the films were exposed to FE-SEM-EDX analysis. Weight and atomic ratio results can be seen in the tables integrated into Fig. 5. In the un-doped CuO film, the

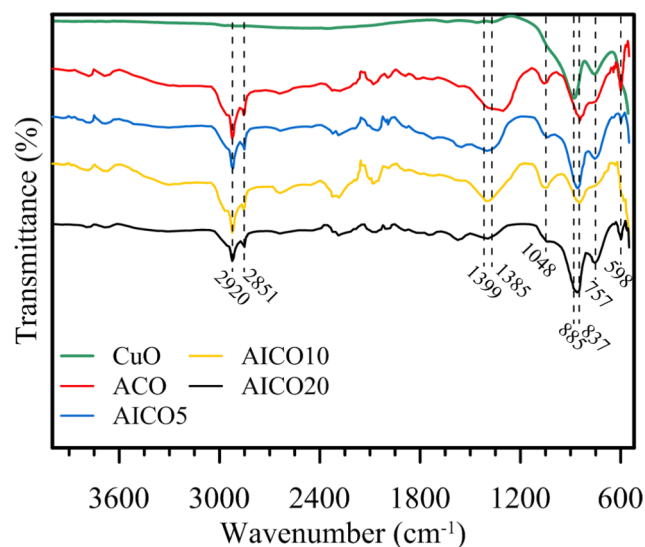


Fig. 7. FTIR spectrum of CuO, ACO and AICO films.

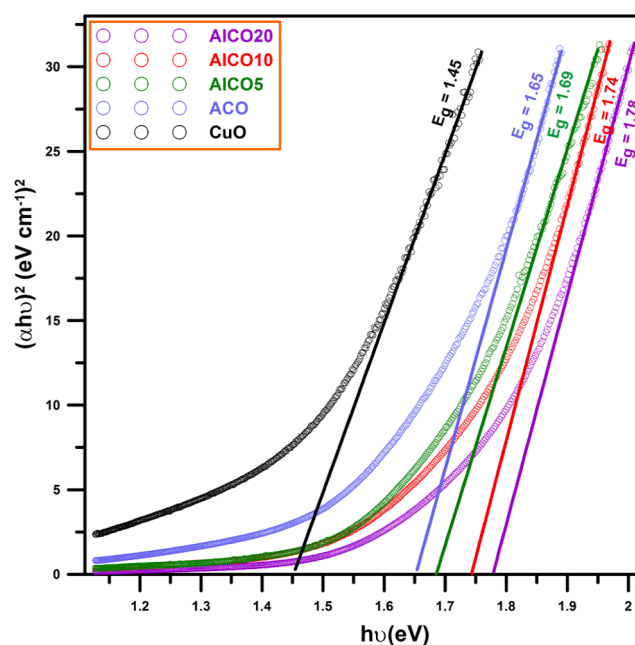


Fig. 8. Estimation of the bandgap of CuO, ACO and AICO films using Tauc's relation.

values of the weight percent of Cu and O are 74.93 and 25.07 respectively. In the AICO5 film, the values of the weight percent of Cu, In, Al, and O are 71.78, 0.39, 0.51, and 27.32, respectively. It can be seen from the mapping images taken from the dual-doped AICO20 film that the colored elements exhibit a homogeneous distribution on the film surface. FE-SEM and mapping images both confirm a successful doping process and show the presence of doped materials.

3.2. Structural analysis

The crystalline phase structure of the CuO films, as functions of the Al and In doping concentration, was designated by X-ray diffraction (XRD). The XRD patterns of the CuO, ACO, and AICO films are indicated in Fig. 6. The recorded peak intensities are summarized in Table 1. The distinct diffraction lines can be listed to the (110), ($\bar{1}11$), (111), (202), (020), (202), ($\bar{1}13$), ($\bar{3}11$), (220), (311), and (004) crystal planes.

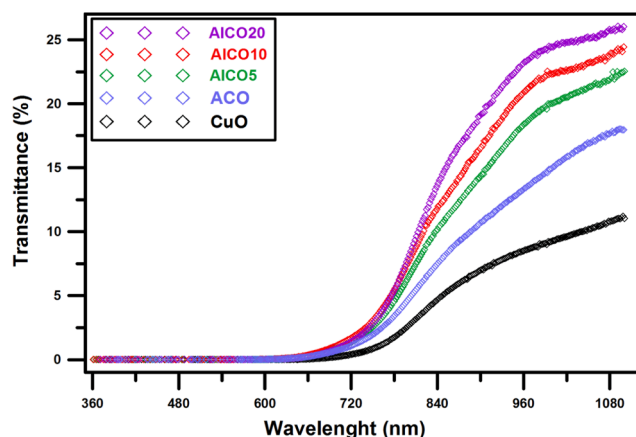


Fig. 9. The optical transmittance spectra of the CuO, ACO and AICO films in 350–1100 nm region.

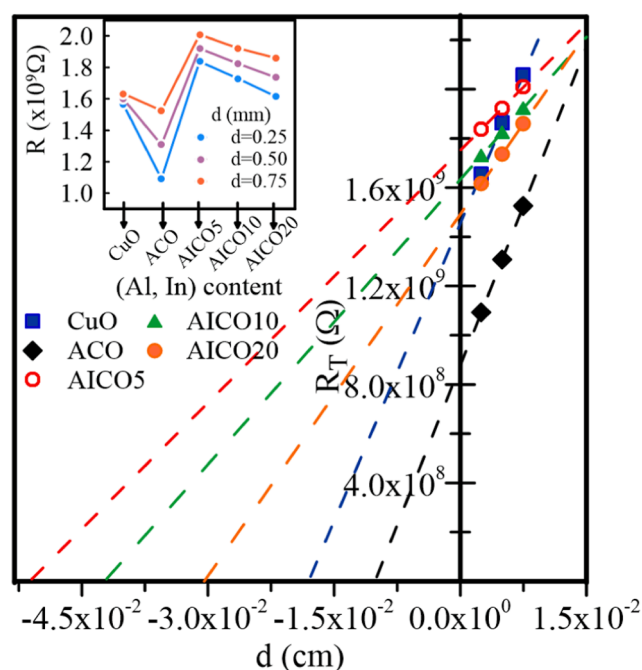


Fig. 10. Calculated resistance (R_T) versus gap spacing (d) plots of CuO, ACO and AICO films. Inset shows the calculated resistivity (R) versus doping percentage of Al and/or In plots.

Between these characteristic peaks, the intense diffraction peaks are located at $2\theta = 35.6^\circ$ and 38.8° with the corresponding planes ($\bar{1}11$) and (111), respectively. All the peaks in the XRD models are compatible with the JCPDS card no: 41–1445. From the XRD spectra, it is observed that the ($\bar{1}11$) and (111) peak intensities are enhanced with the inclusion of an Al source in the solution bath. In addition, as denoted in Fig. 6, the intensity of the ($\bar{1}11$) and (111) diffraction peaks is changed with

Table 2
Calculated resistance values and contact parameters of CuO, ACO and AICO films.

Sample Name	R_1 ($\times 10^9 \Omega$)	R_2 ($\times 10^9 \Omega$)	R_3 ($\times 10^9 \Omega$)	L_T (μm)	ρ_c ($\times 10^6 \Omega\text{cm}^2$)	R_c ($\times 10^9 \Omega$)
CuO	1.564	1.599	1.633	546.1	0.0188	0.765
ACO	1.093	1.309	1.525	50.8	0.0107	0.439
AICO5	1.838	1.921	2.009	256.1	0.0215	0.876
AICO10	1.730	1.825	1.923	211.5	0.0200	0.817
AICO20	1.615	1.736	1.860	152.2	0.0183	0.746

increasing the In doping percentage from 0.5 to 2.0 %.

The intensity of the diffraction peaks in the CuO film is more than in the AICO film because when Al^{3+} and In^{3+} impurities are added, more structural defects occur in the CuO site, leading to stress. The variance in the peak positions due to doping is mainly owing to the various ionic radii of the host Cu^{2+} , Al^{3+} , and In^{3+} dopants. The ionic radius of In^{3+} is greater (0.80 Å) and that of Al^{3+} (0.53 Å) is smaller compared to the ionic radius of the host Cu^{2+} (0.73 Å). Since both the Al^{3+} and In^{3+} ionic radii are different from Cu^{2+} 's, it increases the local tension [23,32,33].

The mean crystallite size values of the prepared CuO, ACO, and AICO films were computed using the Debye-Scherrer's Equation from the X-ray peak broadening. This equation is given as [34,35];

$$D = \frac{0.94\lambda}{\beta \cos\theta} \quad (1)$$

In this formula, D is the mean crystallite size, β , the full-width at half maximum (FWHM) of the obtained peaks in the XRD pattern, θ , the Bragg diffraction angle, and λ , the X-ray wavelength. The crystallite sizes of the samples are summarized in Table 1. The average crystallite size of the CuO film was achieved to be 12.83 nm and that of the 0.5 % Al-doped CuO was 15.10 nm. In addition, when the doping percentage of In is increased the crystallite size rises from 13.85 to 14.65 nm. These variations in crystallite size may be ascribed to the Al^{3+} and In^{3+} ions replacement and incorporated into the CuO lattice matrix [36,37].

3.3. FTIR analysis

FTIR is a useful technique that is used to define the further properties of the grown (doped and un-doped) samples by identifying the characteristic peaks. As shown in Fig. 7, the obtained FTIR spectra of the CuO, ACO, and AICO samples are recorded in the range of $4000\text{--}400\text{ cm}^{-1}$. Metal oxides in general present absorption bands below 1000 cm^{-1} (fingerprint region) owing to the interatomic vibrations. Peaks that appear in the fingerprint region arise from the characteristic stretching vibration mode of the Cu–O bonds [38–40]. Therefore, transmittance peaks at 885 cm^{-1} and 757 cm^{-1} arise from CuO and there are no extraordinary peaks caused by residual starting materials, which were recorded in the un-doped CuO spectrum (Fig. 7). The FTIR patterns of the ACO and AICO films have several absorption peaks. Al and In salts ($(\text{Al}(\text{NO}_3)_3 \cdot 9\text{H}_2\text{O})$ and $(\text{In}(\text{NO}_3)_3 \cdot 3\text{H}_2\text{O})$) were used and some nitrate moiety is shown in the spectrum. Four main vibration modes of nitrate moiety were observed; firstly, an anti-symmetric stretching vibration mode at 1385 cm^{-1} and 1399 cm^{-1} , secondly, a symmetric stretching vibration at 1048 cm^{-1} , thirdly, an out-of-plane deformation vibration at 837 cm^{-1} , and finally, in-plane deformation vibration peaks at 598 cm^{-1} . In addition, the observed peaks between 2000 and 2300 cm^{-1} are the sum of the symmetric stretching vibrations, and peaks between the 2920 and 2851 cm^{-1} sum of the in-plane deformation vibrations [41–43]. With co-doping of Al/In in the CuO films, a somewhat shift in the primary absorption peaks is seen. This could indicate that this minor shift may be related to the changes in Cu–O bond strength [38].

3.4. Optical analysis

The significant optical attributes, like transmittance and bandgap of

the CuO, ACO, and AICO films were searched by using a UV–vis. spectrophotometer. The optical band gaps of the CuO, ACO, and AICO films were computed from the absorbance spectra using a Tauc plot. The bandgaps of these films were estimated using the undermentioned relation [44,45]

$$ah\nu = C(h\nu - E_g)^{1/2} \quad (2)$$

In the formula, ν is the frequency of the photon, h is Planck's constant, α is the absorption coefficient, and E_g is the optical direct bandgap energy. By extrapolating tangent curves to the $h\nu$ axis, the E_g values of the obtained samples are procured and are indicated in Fig. 8. The value of E_g of pure CuO is found to be 1.45 eV, whereas it enhanced to 1.65 eV after Al^{3+} ion doping. This might be due to the microstructural alteration of the CuO samples. The microstructural alteration of the ACO samples could be owing to the substitution of Cu^{2+} interstitial or replacement by Al^{3+} ions [46,47]. In addition, in the AICO films, the increment of In doping percentage (from 0.5 % to 2.0 %) raises the E_g rate from 1.69 eV to 1.78 eV (see Table 1). This increment in the energy bandgap can be clarified as follows: (1) This enhanced bandgap in the blue shift area could be ascribed as owing to modification in the optical bandgap on orbital's hybridization [48]. (2) The bandgap widening may be expounded by the blue shift. This causes the movement of the Fermi level towards the conduction band owing to an increment in electron contents from In ions. Indium atoms supply extra carriers that lead to the shifting of the Fermi level towards the conduction band. For this reason, the band gap becomes bigger [49,50].

The transmittance spectra of the CuO, ACO, and AICO films were examined in the wavelength range of 360 nm–1140 nm, as indicated in Fig. 9. It is obvious from Fig. 9 that these films are highly transparent in the near-infrared (NIR) spectral range. In other words, the films exhibit better optical transmittance in the NIR region. The average transmittance in 700–1100 nm was found to be 10, 16, 23, 25, and 27 % for CuO, ACO, AICO5, AICO10, and AICO20, respectively. Compared to the CuO film, the spectra of the AICO films exhibit significantly improved transmittance in the NIR wavelength region of 900–1100 nm with more than 20–25 % transparency. The optical transmittance of the samples augments with an increase in the In doping percentage.

3.5. Electrical analysis

The TLM method can be used to determine some electrical parameters of thin films based on current–voltage measurements. Specific contact resistance (ρ_c), contact resistance (R_C), and the transfer length (L_T) can be determined from the variation graph of the resistance, depending on the distance between the contacts [51,52]. Furthermore, this method takes the current crowding phenomena into account and the total resistance (R_T) between the pads is given by the following equation [52,53];

$$R_T = \frac{2R_{SK}L_T}{w} + \frac{2R_{SH}l}{w} \quad (3)$$

where w and l are pad width and pad length, and R_{SH} and R_{SK} are altered sheet resistance outside the contact and sheet resistance under the contact, respectively. Values of total resistance can be determined from the linear fit results of the experimental current–voltage (I – V) graphs. Slopes and intercepts of R_T versus gap spacing (d) plot indirectly give the R_C and L_T values of the films (Fig. 10.). The value of ρ_c can be calculated using L_T , estimated from the intersection of the R_T plot for the condition $R_T = 0$ and $d \gg L_T$ in Fig. 10. Hence, the following equation can be written for ρ_c [52,54];

$$\rho_c = R_{SH}L_T^2 \quad (4)$$

Specific contact resistivity values of the CuO films were $0.019 \times 10^6 \Omega \text{cm}^2$ and are compatible with CuO films produced by similar methods in the literature [40,53,54]. The lowest value of specific

contact resistivity was $0.011 \times 10^6 \Omega \text{cm}^2$ and achieved by ACO (Al: 0.5 %) (Table 2). These results show that the specific contact resistivity value was slightly decreased with the doping of aluminum but indium co-doping increased these values, and when the indium doping ratio increased, this value slightly decreased (inset in Fig. 10). This dependency on the doping percentage of Al and/or In can be explained by not only the influence of some morphological parameters (e.g. film quality, particle distribution, and size surface roughness, etc.) but also by an increase in the local tension due to the ionic radius of In^{3+} [55,56].

4. Conclusion

In this work, bare CuO, ACO, and AICO films were obtained on soda-lime glass substrates via the cost-effective SILAR method. The film's physical properties, like surface morphological, structural, optical, and electrical were examined, concerning alterations in the Al dopant and In co-dopants concentration. FE-SEM images illustrated that the surface morphologies of the obtained films were remarkably varied by the Al doping and Al and In co-doping. The EDX results confirmed that Al and In impurities were appropriately added to the lattice structure of CuO. The XRD results displayed that all the CuO films were of polycrystalline structure and no characteristic peaks from Al and In impurities were detected. The FTIR spectrum affirmed the CuO stretching vibration bond. The UV–vis spectra of the films demonstrated a blue shift in the absorption spectra compared with bulk CuO. Optical analyses showed that the transmittance of CuO films increased with Al and In doping. From these results, we deduce that ACO and AICO films are good candidates for optoelectronic applications.

Data availability

The authors confirm that all data generated or analyzed during this study are included in this published article.

CRediT authorship contribution statement

O. Kahveci: Investigation, Data curation, Writing – review & editing. **A. Akkaya:** Data curation, Writing – review & editing. **R. Aydin:** Investigation, Methodology, Formal analysis, Data curation, Writing – review & editing, Supervision. **B. Şahin:** Investigation, Methodology, Data curation, Writing – review & editing. **E. Ayyıldız:** Data curation, Supervision.

Declaration of Competing Interest

The authors declare that they have no known competing financial interests or personal relationships that could have appeared to influence the work reported in this paper.

Data availability

No data was used for the research described in the article.

References

- [1] S. Kumar, F.A. Alharthi, A. El marghany, F. Ahmed, N. Ahmad, K.H. Chae, K. Kumari, Role of Fe doping on surface morphology, electronic structure and magnetic properties of Fe doped CeO_2 thin film, *Ceram. Int.*, 47 (2021) 4012–4019.
- [2] T.M.S. Dawoud, V. Pavitra, P. Ahmad, A. Syed, G. Nagaraju, Photocatalytic degradation of an organic dye using Ag doped ZrO_2 nanoparticles: Milk powder facilitated eco-friendly synthesis, *J. King Saud Univ. – Sci.* 32 (2020) 1872–1878.
- [3] M.A. Sayeed, H.K. Rouf, Al-doped SnO_2 thin films: impacts of high temperature annealing on the structural, optical and electrical properties, *J. Mater. Res. Technol.* 15 (2021) 3409–3425.
- [4] A.M. Abdallah, M. Noun, R. Awad, Tuning the structural, optical and magnetic properties of PVP-capped NiO nanoparticles by gadolinium doping, *Appl. Phys. A* 127 (2021) 760.

- [5] M. Mumtaz, M. Ahsan Mahmood, S.D. Khan, M. Aslam Zia, A. Iqbal, M. Ahmed, I. Ahmad, Optical and conductive properties of Antimony-Bismuth co-doped titanium dioxide in terahertz range, *Infrared Phys. Techn.* 112 (2021), 103570.
- [6] S. Velliyan, V. Rajendran, Study on the effect of Ce³⁺ doping on structural, morphological and optical properties of CuO nanoparticles synthesized via combustion technique, *Phys. B Condens. Matter* 613 (2021), 413015.
- [7] A. Badawi, S.S. Alharthi, M.G. Althobaiti, A.N. Alharbi, H. Assaedi, H. I. Alkhamash, N. Al-Hosiny, Structure investigation and optical bandgap tuning of La-doped CuO nanostructured films prepared by spray pyrolysis technique, *Appl. Phys. A* 127 (2021) 235.
- [8] S.P. Kamble, V.D. Mote, Optical and room-temperature ferromagnetic properties of Ni-doped CuO nanocrystals prepared via auto-combustion method, *J. Mater. Sci. Mater. Electron.* 32 (2021) 5309–5315.
- [9] H. Siddiqui, M.R. Parra, P. Pandey, M.S. Qureshi, F.Z. Haque, Utility of copper oxide nanoparticles (CuO-NPs) as efficient electron donor material in bulk-heterojunction solar cells with enhanced power conversion efficiency, *J. Sci.: Adv. Mater. Devices* 5 (2020) 104–110.
- [10] Y. Yang, J. Yang, W. Yin, F. Huang, A. Cui, D. Zhang, W. Li, Z. Hu, J. Chu, Annealing time modulated the film microstructures and electrical properties of P-type CuO field effect transistors, *Appl. Surf. Sci.* 481 (2019) 632–636.
- [11] E. Yuan, P. Ni, W. Zhuang, R. Jian, P. Jian, Synergic catalysis by a CuO-like phase and CuO for anaerobic dehydrogenation of 2,3-butanediol, *J. Catal.* 382 (2020) 256–268.
- [12] S. Moshleh, M.R. Rahimi, M. Ghaedi, K. Dashtian, S. Hajati, Sonochemical-assisted synthesis of CuO/Cu₂O/Cu nanoparticles as efficient photocatalyst for simultaneous degradation of pollutant dyes in rotating packed bed reactor: LED illumination and central composite design optimization, *Ultrason. Sonochem.* 40 (2018) 601–610.
- [13] J. Uddin, M. Sharmin, M.N. Hasan, J. Podder, Influence of Ni doping on the morphological, structural, optical and electrical properties of CuO thin films deposited via a spray pyrolysis, *Opt. Mater.* 119 (2021), 111388.
- [14] R. Jana, A. Dey, M. Das, J. Datta, P. Das, P.P. Ray, Improving performance of device made up of CuO nanoparticles synthesized by hydrothermal over the reflux method, *Appl. Surf. Sci.* 452 (2018) 155–164.
- [15] C.M. Muiva, A.O. Juma, L.M. Lepodise, K. Maabong, D. Letsholathebe, Surfactant assisted chemical bath deposition based synthesis of 1-D nanostructured CuO thin films from alkaline baths, *Mat. Sci. Semicon. Proc.* 67 (2017) 69–74.
- [16] H.E. Aakib, J.F. Pierson, L. Atourki, L. Nkhaili, A.E. Kissani, A. Narjis, A. Outzourhit, Preparation and characterization of nanocomposite of Co:CuO by radio-frequency sputtering for solar selective absorber application, *Thin Solid Films* 709 (2020), 138199.
- [17] O. Daoudi, A. Elmadani, M. Lharch, M. Fahoume, A new efficient synthesis of CuO thin films using modified SILAR method, *Opt. Quant. Electron.* 52 (2020) 1–17.
- [18] I.A. Zgair, A.H. Omran Alkhatay, A.A. Muhmood, S.K. Hussain, Investigation of structure, optical and photoluminescence characteristics of Li doped CuO nanostructure thin films synthesized by SILAR method, *Optik* 191 (2019) 48–54.
- [19] M. Hjiri, M.S. Aida, O.M. Lemine, L. El Mir, Study of defects in Li-doped ZnO thin films, *Mat. Sci. Semicon. Proc.* 89 (2019) 149–153.
- [20] M.I. Khan, A. Suleman, M.S. Hasan, S.S. Ali, T.I. Al-Muhimeed, A.A. AlObaid, M. Iqbal, M.M. Almonneef, N. Alwadai, Effect of Ce doping on the structural, optical, and photovoltaic properties of TiO₂ based dye-sensitized solar cells, *Mater. Chem. Phys.* 274 (2021), 125177.
- [21] W.Z. Tawfik, Z.S. Khalifa, M.S. Abdel-wahab, A.H. Hammad, Sputtered cobalt doped CuO nano-structured thin films for photoconductive sensors, *J. Mater. Sci. Mater. Electron.* 30 (2019) 1275–1281.
- [22] M.R. Islam, J.E. Obaid, M. Saiduzzaman, S.S. Nishat, T. Debnath, A. Kabir, Effect of Al doping on the structural and optical properties of CuO nanoparticles prepared by solution combustion method: Experiment and DFT investigation, *J. Phys. Chem. Solid* 147 (2020), 109646.
- [23] A. Sukee, E. Kantarak, P. Singjai, Preparation of Aluminum doped Zinc Oxide Thin Films on Glass Substrate by Sparking Process and Their Optical and Electrical Properties, *J. Phys. Conf. Ser.* 901 (2017), 012153.
- [24] A. Djeghlouf, D. Hamri, A. Teffahi, A. Saidane, F.S. Al Mashary, M.M. Al Huwayz, M. Henini, I. Orak, A.M. Albadri, A.Y. Alyamani, Effect of indium doping on the electrical and structural properties of TiO₂ thin films used in MOS devices, *J. Alloy. Compd.* 775 (2019) 202–213.
- [25] K. Tang, S. Gu, J. Liu, J. Ye, S. Zhu, Y. Zheng, Effects of indium doping on the crystallographic, morphological, electrical, and optical properties of highly crystalline ZnO films, *J. Alloy. Compd.* 653 (2015) 643–648.
- [26] A. Akkaya, E. Ayyıldız, Automation Software for Semiconductor Research Laboratories: Electrical Parameter Calculation Program (SeCLaS-PC), *J. Circ., Syst. Comput.* 29 (2020) 2050215.
- [27] A. Akkaya, E. Ayyıldız, Automation Software for Semiconductor Research Laboratories: Measurement System and Instrument Control Program (SeCLaS-IC), *Mapan* 35 (2020) 343–350.
- [28] B. Şahin, T. Kaya, Enhanced hydration detection properties of nanostructured CuO films by annealing, *Microelectron. Eng.* 164 (2016) 88–92.
- [29] S. Syed Zahirullah, P. Immanuel, S. Pravinraj, P. Fermi Hilbert Inbaraj, J. Joseph Prince, Synthesis and characterization of Bi doped ZnO thin films using SILAR method for ethanol sensor, *Mater. Lett.* 230 (2018) 1–4.
- [30] B. Şahin, Dual doping (Cu with rare-earth element Ce): An effective method to enhance the main physical properties of CdO films, *Superlattice. Microsc.* 136 (2019), 106296.
- [31] A. Akkaya, B. Şahin, R. Aydın, H. Çetin, E. Ayyıldız, Solution-processed nanostructured ZnO/CuO composite films and improvement its physical properties by lustrous transition metal silver doping, *J. Mater. Sci. Mater. Electron.* 31 (2020) 14400–14410.
- [32] J.H. Lim, S.M. Lee, H.-S. Kim, H.Y. Kim, J. Park, S.-B. Jung, G.C. Park, J. Kim, J. Joo, Synergistic effect of Indium and Gallium co-doping on growth behavior and physical properties of hydrothermally grown ZnO nanorods, *Sci. Rep.-UK 7* (2017) 41992.
- [33] S. Alamdari, M. Tafreshi, M.S. Ghamsari, Strong yellow-orange emission from aluminum and Indium co-doped ZnO nanostructures with potential for increasing the color gamut of displays, *Appl. Phys. A* 125 (2019) 165.
- [34] A. Tasdemir, R. Aydın, A. Akkaya, N. Akman, Y. Altınay, H. Cetin, B. Sahin, A. Uzun, E. Ayyıldız, A green approach for the preparation of nanostructured zinc oxide: Characterization and promising antibacterial behaviour, *Ceram. Int.* 47 (2021) 19362–19373.
- [35] B.D. Cullity, Elements of X-Ray Diffraction, *Am. J. Phys* 25 (1957) 394–395.
- [36] A. Hadri, C. Nassiri, F. Chafi, M. Lohgmarti, B. Fares, L. Laanab, F. Chraïbi, M. Bensitel, A. Mzred, Indium Doping Effect on Structural, Optical and Electrical Properties of Sprayed ZnO Thin Films, *Sens. Transducers* 178 (2014) 63.
- [37] T. Jan, S. Azmat, Q. Mansoor, S. Ilyas, I. Ahmad, H. Khan, M. Ismail, Structural, Raman, optical and novel antibacterial characteristics of Al doped CuO nanostructures, *Mater. Res. Express* 6 (2019) 1050a1053.
- [38] N. Thakur, K.K. Anu, Effect of (Ag, Co) co-doping on the structural and antibacterial efficiency of CuO nanoparticles: A rapid microwave assisted method, *Journal of Environmental, Chem. Eng.* 8 (2020), 104011.
- [39] S. Iqbal, M. Javed, A. Bahadur, M.A. Qamar, M. Ahmad, M. Shoaib, M. Raheel, N. Ahmad, M.B. Akbar, H. Li, Controlled synthesis of Ag-doped CuO nanoparticles as a core with poly(acrylic acid) microgel shell for efficient removal of methylene blue under visible light, *J. Mater. Sci. Mater. Electron.* 31 (2020) 8423–8435.
- [40] A. Akkaya, O. Kahveci, R. Aydın, B. Şahin, Amplifying main physical characteristics of CuO films using ascorbic acid as the reducer and stabilizer agent, *Appl. Phys. A* 127 (2021) 911.
- [41] N. He, Y. Ni, J. Teng, H. Li, L. Yao, P. Zhao, Identification of inorganic oxidizing salts in homemade explosives using Fourier transform infrared spectroscopy, *Spectrochim. Acta A Mol. Biomol. Spectrosc.* 221 (2019), 117164.
- [42] I.F. Myronyuk, V.I. Mandzyuk, V.M. Sachko, V.M. Gun'ko, Structural and Morphological Features of Disperse Alumina Synthesized Using Aluminum Nitrate Nonahydrate, *Nanoscale Res. Lett.*, 11 (2016) 153.
- [43] E. El-Shereafy, M.M. Abousekkina, A. Mashaly, M. El-Ashry, Mechanism of thermal decomposition and γ -pyrolysis of aluminum nitrate nonahydrate [Al(NO₃)₃·9H₂O], *J Radioanal Nucl Ch* 237 (1998) 183–186.
- [44] B. Şahin, R. Aydın, H. Cetin, Variation of the key morphological, structural, optical and electrical properties of SILAR CdO with alkaline earth Ca²⁺ ions doping, *Ceram. Int.* 45 (2019) 16748–16758.
- [45] J. Tauc, *Amorphous and liquid semiconductors*, Plenum Press, New York, 1974.
- [46] M. Shirazi, R. Sabet Dariani, M.R. Toroghinejad, Influence of doping behavior of Al on nanostructure, morphology and optoelectronic properties of Al Doped ZnO thin film grown on FTO substrate, *J. Mater. Sci. Mater. Electron.* 27 (2016) 10226–10236.
- [47] M. Arfan, D.N. Siddiqui, T. Shahid, Z. Iqbal, Y. Majeed, I. Akram, R. Noreen, Z. Bagheri, A.Z. Song, Tailoring of nanostructures: Al doped CuO synthesized by composite-hydroxide-mediated approach, *Results Phys.* 13 (2019), 102187.
- [48] A. Dhanalakshmi, B. Natarajan, V. Ramadas, Effect of Cobalt Incorporation on Structural, Morphological, Optical and Antibacterial Properties of Rod Shaped ZnO Nanoparticles, in *Springer International Publishing, Cham*, 2017, pp. 205–217.
- [49] T. Tohsophon, N. Wattanasupinyo, B. Silskulsuk, N. Sirikulrat, Effect of aluminum and indium co-doping on zinc oxide films prepared by dc magnetron sputtering, *Thin Solid Films* 520 (2011) 726–729.
- [50] M.J. Akhtar, H.A. Alhadlaq, A. Alshamsan, M.A. Majeed Khan, M. Ahamed, Aluminum doping tunes band gap energy level as well as oxidative stress-mediated cytotoxicity of ZnO nanoparticles in MCF-7 cells, *Sci. Rep.-UK 5* (2015) 13876.
- [51] D.K. Schroder, *Semiconductor Material And Device Characterization*, John Wiley & Sons, New York, 2006.
- [52] G.K. Reeves, H.B. Harrison, Obtaining the Specific Contact Resistance from Transmission-Line Model Measurements, *Electron Devic. Lett.* 3 (1982) 111–113.
- [53] H. Çavuşoğlu, R. Aydın, Complexing agent triethanolamine mediated synthesis of nanocrystalline CuO thin films at room temperature via SILAR technique, *Superlattice. Microsc.* 128 (2019) 37–47.
- [54] L. De Los Santos, D.H. Valladares, A.B. Salinas, D.A. Dominguez, S.I. Najarro, T. Khondaker, C.H.W. Mitrelias, J.A. Barnes, Y.M. Aguiar, Crystallization and electrical resistivity of Cu₂O and CuO obtained by thermal oxidation of Cu thin films on SiO₂/Si substrates, *Thin Solid Films* 520 (2012) 6368–6374.
- [55] A. Pramotheekumar, N. Senthilkumar, K.C. Mercy Gnana Malar, M. Meena, I. Vetha Potheher, A comparative analysis on the dye degradation efficiency of pure, Co, Ni and Mn-doped CuO nanoparticles, *J. Mater. Sci.: Mater. Electron.* 30 (2019) 19043–19059.
- [56] N. Ahmad, S. Khan, Effect of (Mn-Co) co-doping on the structural, morphological, optical, photoluminescence and electrical properties of SnO₂, *J. Alloy. Compd.* 720 (2017) 502–509.